inter.noise 2014
MELBOURNE AUSTRALIA
16-19 NOVEMBER

Development of the Microphone-Array Measurement Technique for use in Cryogenic and Pressurized Wind Tunnels

Thomas AHLEFELDT[1]; Carsten SPEHR[1]

[1] German Aerospace Center, Germany

ABSTRACT

In the development process of aircrafts and rail vehicles, the use of microphone phased arrays to acquire acoustic data on scaled models in conventional wind tunnels has become feasible. Since conventional wind tunnels cannot generally achieve full-scale Reynolds numbers, aerodynamic measurements are performed in cryogenic and/or pressurized wind tunnels which are capable of full-scale/higher Reynolds number flows. The microphone array measurement technique has been further developed for the use in cryogenic (down to 100 K) and pressurized (up to 450 kPa) wind tunnels.
The comparison of aeroacoustic results obtained from wind tunnel tests with results from real flight tests shows differences. The differences can be attributed to lack of model-fidelity, installation effects, the Reynolds number and the assumptions made in phased array processing. This work focuses on the effect of the Reynolds number.
This paper gives an overview of the efforts at to make microphone array measurement technique available to use in pressurized and cryogenic condition. The aim of this development is to enable acoustic measurements on scaled aircraft models in start and landing configuration at real-flight Reynolds numbers.

Keywords: Reynolds number, microphone array, subsonic flow, aircraft noise, small scale model, wind tunnel, elastic deformation I-INCE Classification of Subjects Number(s): 74.7

INTRODUCTION

The development process of aircraft and rail vehicles is so expensive and time consuming that uncertainties attached to the future performance of the vehicle shall be minimized. To evaluate the acoustic performance the use of microphone phased arrays to acquire acoustic data on scaled models in conventional wind tunnels with closed test section has become feasible and mainstream. The acoustically relevant flight conditions are the landing configuration at relatively small Mach-Numbers. Conventional wind tunnels cannot generally achieve full-scale Reynolds numbers of aircrafts in landing configurations. Aerodynamic measurements are therefore performed in cryogenic and/or pressurized wind tunnels. The aim of the current development at the DLR is to combine these expensive but necessary measurements with microphone array measurements. For this purpose the microphone array measurement technique has been further developed for the use in cryogenic (down to 100 K) and pressurized (up to 450 kPa) wind tunnels. Stoker(1) has shown that the aeroacoustic results obtained from wind tunnel tests differs from real flight test. The differences can be caused by different reasons like the installation effects of the model in the wind tunnel, geometrical differences between model and real aircraft, the Reynolds number and the in the phased array processing(2). This work focuses on identifying and avoiding effects of the Reynolds number. This proceeding summarizes the state of the work on aeroacoustic measurements in cryogenic/pressurized wind tunnels. For more information see Ahlefeldt et al.(3, 4, 5, 6).

OVERVIEW OF TESTS IN CRYOGENIC/PRESSURIZED CONDITIONS

The test in cryogenic and pressurized conditions were performed in four steps.

1. The aim of the first step was the proof of concept of aeroacoustic measurements under cryogenic conditions. These tests were performed at the DNW-KKK (Kryo-Kanal Koeln) at ambient pressure using a circular cylinder as an aeroacoustic noise source with known Reynolds number dependency. The focus of these experiments lay on the technical challenges to measure at temperatures down to 100 K with

[1] Thomas.Ahlefeldt@dlr.de
[2] Carsten.Spehr@dlr.de

special attention to the calibration of the microphones under cryogenic conditions.
2. The second step - again at ambient pressure conditions - was a demonstration experiment using an aircraft half-model as an typical application. These measurements were performed again at the DNW-KKK up to 40% of the real-flight Reynolds number based on the mean aerodynamic chord.
3. These two experiments were the basis of the third experiment, where the measurement technique has been further developed to use in cryogenic and pressurized conditions. These test were performed in the PETW, a small scale wind tunnel for preliminary testing at the European Transonic Windtunnel (ETW) site, on a cylinder as the aeroacoustic source. Again the focus lay on the performance of acoustic measurement equipment under cryogenic and pressurized condition especially on the calibration.
4. For the time being, the last stage in development of microphone array measurement technique was a demonstration experiment on a scaled half-model in the ETW itself. The aim of this experiment among to demonstrate of availability of microphone array measurement technique for industrial application, was to investigate whether a Reynolds number dependency of scaled aircraft models can be sustained and whether these effects can be distinguished from effect of different elastic deformation under cryogenic conditions. To our knowledge, this is the first experiment which acquire airframe noise data of a scaled model at real-flight Reynolds numbers.

DATA PROCESSING

The signals of the microphone array were sampled simultaneously by a data acquisition system located outside the test sections with an A/D conversion of 16 bits. The array data were processed using the beamforming algorithm in the frequency domain to obtain the reconstructed source auto-powers $\hat{S}_{exp}$ on a grid at scan locations $\mathbf{y_f}$:

$$\hat{S}_{exp}(\mathbf{y}_f, \omega) = \mathbf{e}^{\mathscr{H}} \mathbf{R}_{DR} \mathbf{e}. \tag{1}$$

$\mathbf{R}_{DR}$ denotes the cross-correlation matrix of the microphone signals dependent on frequency ω. The subindex *DR* denotes that the diagonal term of the cross correlation matrix $\mathbf{R}$ has been set to zero. The phasor $\mathbf{e}$ describes the relevant phase shift based on the point source assumption under homogeneous flow conditions. Additionally, $\mathbf{e}$ incorporates distance scaling in terms of sensor weighting. This was performed using the conventional beamforming approach(7) which leads to a relative weighting of the sensors to each other which is inversely proportional to the source distance from the sensor. $\mathscr{H}$ denotes the conjugate transpose.

Condition Correction

In a cryogenic and pressurized test section the acquired data are dependent on the different temperatures and pressures in the test section. For comparability, the influence of those quantities must be considered in terms of a correction. The evaluation of the measurements leads to a data set of sound pressures depending on the density ρ, the Mach number M, and the speed of sound a. Assuming a perfect gas, its density is described by the ideal gas law:

$$\rho = \frac{p}{\mathscr{R}T}. \tag{2}$$

The speed of sound is given by:

$$a(p,T) = \sqrt{\frac{\gamma(p,T)\mathscr{R}T}{m_{mol}}}. \tag{3}$$

$\mathscr{R}$ denotes the molar gas constant and m_{mol} the molar mass, both constant for pure nitrogen. The slight change of the adiabatic γ in the examined pressure and temperature range can for example be obtained from tabulation(8). Both quantities, ρ and a, depend on the static pressure and the temperature and affect the radiated sound pressure. Most often, airframe noise sources can be modeled as dipoles(9, 10, 11, 12). As shown by Curle(13), the sound generated in the far-field for compact dipole sources at low Mach numbers is of order

$$I \propto \rho a^{-3} u_\infty^6. \tag{4}$$

With the intensity in the farfield $I = \overline{p'^2}/\rho a$, the square acoustic pressure of the noise radiated is of order

$$\overline{p'^2} \propto \rho^2 a^{-2} u_\infty^6, \tag{5}$$

or, in terms of the Mach number:

$$\overline{p'^2} \propto \rho^2 a^4 M^6. \tag{6}$$

For a constant Mach number the decibel correction for dipole sources considering the different temperatures and static pressures in the test section is calculated by:

$$\Delta dB = 10\log_{20}\left(\frac{\rho a^2}{\rho_0 a_0^2}\right) \tag{7}$$

with $\rho_0 = 1.25\,\mathrm{kg/m^3}$ and $a_0 = 337\,\mathrm{m/s}$ (c and ρ for pure nitrogen at standard conditions $p_0 = 101325$ Pa and $T_0 = 273.15$ K). With the help of equation 7 the data acquired at different pressures and temperatures can be normalized.

MEASUREMENTS ON A CIRCULAR CYLINDER AT DNW-KKK

Microphone Array

Measurements in cryogenic environment place particular requirements on sensor equipment and the fairing of the microphone array. In a primary step, different microphones, electronic devices, cables for signal and fairing materials were tested at cryogenic temperatures. For the microphones, simple electret microphones of type RTI 1207A shown to be capable of surviving cryogenic test conditions temperatures down to 100 K. For the electronic devices such as the self-built preamplifier cryogenic-capable components were chosen, and the cables were coated with Teflon. The microphone array fairings were made of an aluminum alloy. To allow for contraction of the alloy at lower temperatures, the fairing assemblies were rigidly fixed only at the center.
In a second step a linear microphone-array suitable for cryogenic testing and consisting of 21 microphones (arranged at logarithmic distances) was constructed. This prototype array was used for the tests on the circular cylinder(3).

Calibration Procedure

In terms of frequency response at standard conditions ($T \approx 290$ K) for the individual microphones mounted in the arrays, comparative calibrations with a $\frac{1}{4}$-inch G.R.A.S. condenser microphone were carried out in a semi-anechoic chamber prior to the measurement. The phase matching of the microphones was checked using a cross-correlation analysis, with a calibration source at known positions.
The frequency response at different temperatures must also be determined. The type of electret microphone used was compared to prototype $\frac{1}{4}$-inch Brüel&Kjær cryogenic condenser microphones with a known temperature-amplitude response to obtain the temperature dependent frequency response. Figure 1 shows the frequency response (normalized to that of $T = 290$ K) of the electret microphones for several temperatures. The amplitude correction was applied to all measured data.

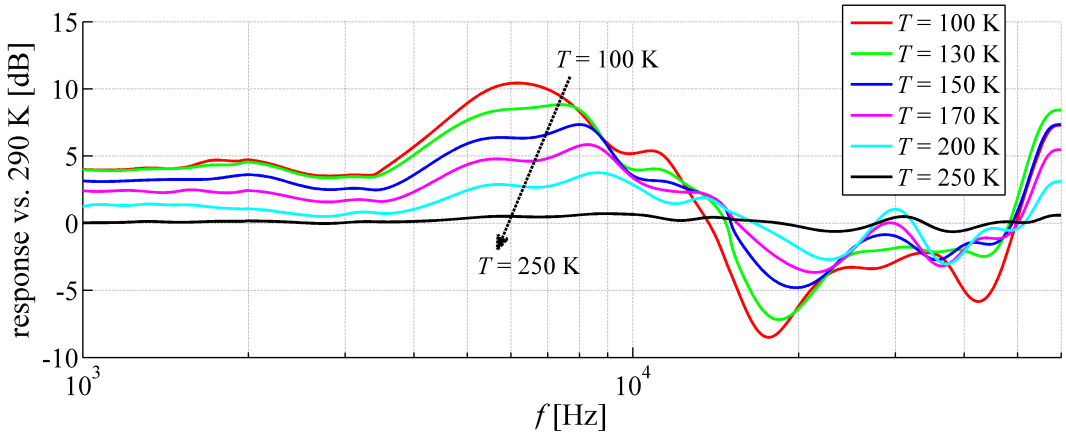

Figure 1 – Frequency response (dB) (normalized to that of 290 K) of the electret microphones used in the microphone array for several temperatures from 100 K to 250 K.

Measurements and Results

The measurements with the prototype microphone-array were performed at the DNW-KKK. For the measurement setup a circular cylinder ($d = 2.5$ mm) was used as an aeroacoustic noise source. Measurements were carried out with a wide range of the Mach number (0.1 to 0.3) and the temperature (290 K to 100 K) leading to a range of the Reynolds number (based on the cylinder diameter) from $5 \cdot 10^3$ to $4 \cdot 10^4$. Each calculated spectrum showed a peak maximum at the cylinder's vortex shedding frequency. The sound power

level of those peaks were compared to a prediction model(14), which is based on the noise radiation from a circular cylinder in a homogeneous flow field. The resulting sound power P_{pred} depends on the state of the surrounding fluid (ρ-density, c_0-speed of sound, u_∞-free stream velocity) and on quantities dependent on the Reynolds number:

$$P_{pred} \propto \rho c_0^{-3} u_\infty^6 St^2 C_{l'}^2 \Lambda_d \tag{8}$$

The Reynolds number dependent quantities are the Strouhal number St, the fluctuating lift coefficient $C_{l'}$ and the correlation length Λ_d. These data have not been separately determined in the present study, so empirical data from literature has been used(15). Figure 2 shows a very good agreement between the measured data and the prediction model. Deviations can be identified at low Mach numbers and at specific Reynolds numbers. They can mostly be attributed to a low signal-to-noise ratio (at low Mach numbers), uncertainties in the temperature-dependent amplitude calibration, a temperature and velocity dependent turbulence level in the test section and hysteresis effects.

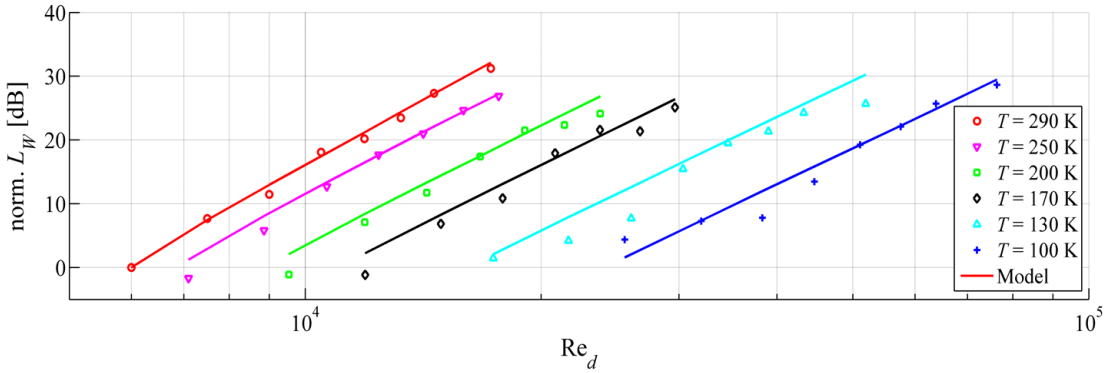

Figure 2 – Comparison of the measured results (•) with the model (—) at different temperatures plotted versus the Reynolds number.

MEASUREMENTS ON A DO-728 HALF MODEL AT THE DNW-KKK

Microphone Array

Based on the linar prototype array use for the tests on the circular cylinder, a large microphone-array containing 144 electret microphones was built. The dimensions of the array are 1756 mm in streamwise and 1300 mm in vertical (normal to the flow) direction. The array protrudes 25 mm into the test section. The microphones are arranged in spiral arms. This array was used for the measurements on the DO-728 half-model(5).

Calibration Procedure

For the large 144 microphone array the same electret microphones with the afore mentioned temperature dependent frequency response were used.

Measurements and Results

With the large microphone-array acoustic measurements on a 9.24% Dornier-728 half-model were performed at the DNW-KKK. Measurements were carried out within a wide range of operational flow parameters. The angles of attack were varied from -2° to 10° , the temperature from 100 K to 290 K and the Mach number from 0.125 to 0.25. The range of the Reynolds number was $1 \cdot 10^6$ to $9 \cdot 10^6$, where the Reynolds number is based on the mean aerodynamic chord length of 353 mm and the free stream velocity of the uniform flow. Figure 3 shows a photo of the measurement setup.

Figure 4 shows the comparison for a Mach number of 0.2 and an angle of attack of 3° for different Strouhal numbers (based on the mean aerodynamic chord length). The source maps on the left are obtained from measurements at 290 K and that on the right side at 100 K. At a Strouhal number of 25 the comparison shows almost the same map, the sound sources are almost equal in location and source strength. With a Strouhal number of 50 the maps show slight differences. The flap-tip noise dominates both maps, but the sources on the slat are weaker at the higher Reynolds number. Surprisingly, at $Re = 7.2 \cdot 10^6$ for a Strouhal number of 100 one sees a noise source on the nacelle-strake, which dominates the source map. The source maps at a Strouhal number of 200 show almost the same result for the different Reynolds numbers, but for the lower Reynolds number the slat noise in the vicinity of the nacelle is increased.

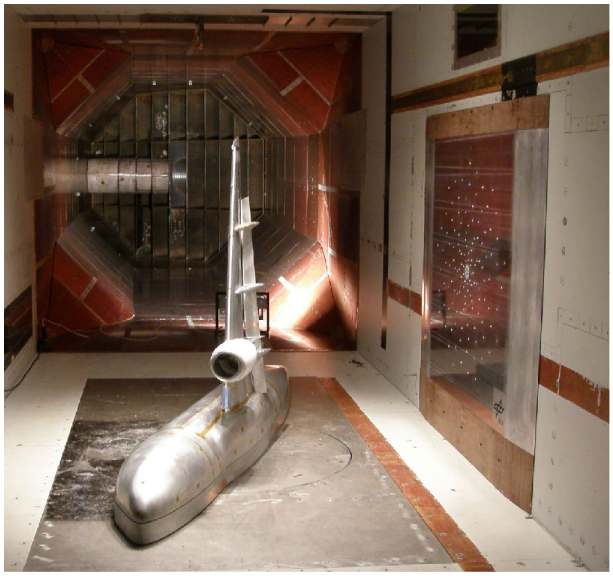

Figure 3 – Photo of the measurement setup with the array mounted on the side wall and the DO-728 half-model in the centre of the test section.

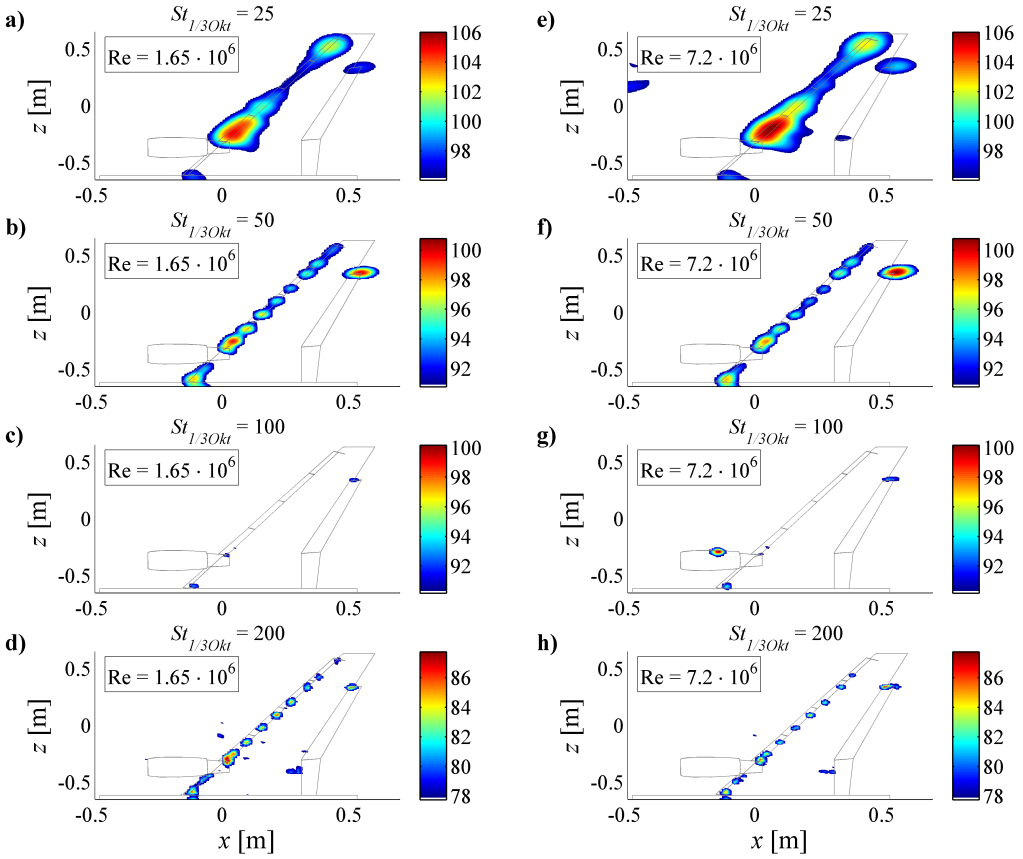

Figure 4 – Comparison of the source maps at $M = 0.20$ and $\alpha = 3°$ for $T = 290$ K (a-d) and $T = 100$ K (e-h). The corresponding Reynolds numbers are $1.65 \cdot 10^6$ and $7.20 \cdot 10^6$. Displayed are the 3rd-octave band results with the centre Strouhal numbers St_δ = 25, 50, 100 and 200. The range of colour scales is always 10 dB, the maximum level is that appropriate for each Strouhal number case.

TESTS ON A CIRCULAR CYLINDER AT PETW

Microphone Array

For the PETW measurements, a microphone array suitable for cryogenic and pressurized testing consisting of 12 microphones was constructed. The $\frac{1}{4}$-inch Brüel&Kjær cryogenic condenser microphones were used. A dummy window plate (aluminum) of the PETW test section was used for the installation of the microphones. The microphones were arranged on two arcs and spaced at logarithmic distances(4).

Calibration procedure

The calibration measurement was performed using four of the $\frac{1}{4}$-inch Brüel&Kjær cryogenic condenser microphones of type 4944A. The frequency response was measured in the range from 500 Hz to 100 kHz under combined cryogenic and pressurized conditions. An excitation signal was simulated by electrostatic actuators in the cryogenic vessel of the ETW. The static pressure was varied in six steps from 110 kPa to 450 kPa and the temperature was altered in 7 steps in the range of 290 K to 120 K. The temperature was obtained via PT100-sensors mounted on the microphones. The combined influence of the non-ambient static pressure and non-ambient temperature on the frequency response can be seen in figure 5. The amplitude response varies strongly with frequency and the wavy shape of the response curves show maxima and minima that go from -20 dB to $+9$ dB. The comparison to results obtained at various temperatures and ambient pressure e.g. at various pressures and ambient temperature (not shown here, see (4)) demonstrated that temperature and static pressure dependencies of the frequency response are mutually dependent on each other.

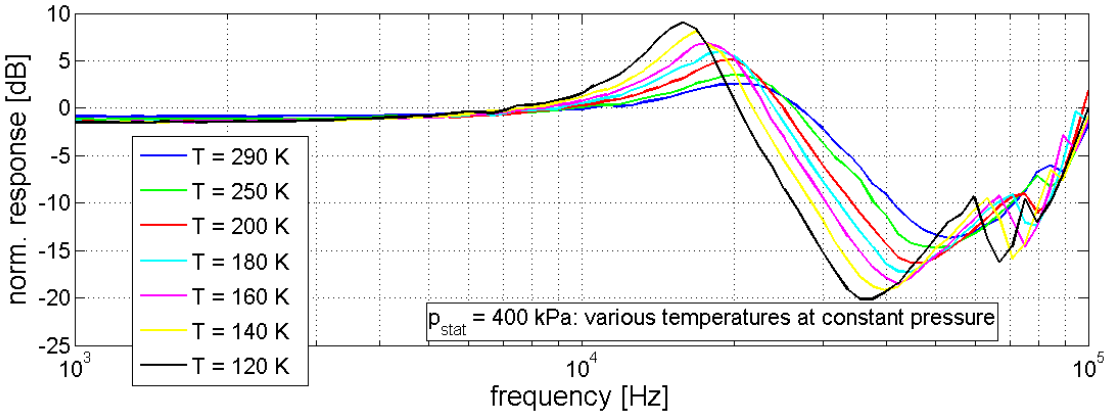

Figure 5 – Frequency response of the Brüel&Kjær 4944A cryogenic pressure-field 1/4-inch microphones at 400 kPa and various temperatures. The results are normalized to the frequency response at 110 kPa and 290 K.

Measurements and Results

For the measurement setup at the PETW a circular cylinder with a diameter of 2 mm was used as an aeroacoustic noise source. The temperature and static pressure were varied in the range 120 K to 290 K and 110 kPa to 400 kPa, respectively. The Mach number was altered in the range of 0.15 to 0.3, leading to a range of the Reynolds number (based on the cylinder diameter) from $7.6 \cdot 10^3$ to $1.9 \cdot 10^5$. Additionally the decibel correction was used (equation 7), to take account of the pressure and temperature effect in the test section on the radiated noise from the cylinder. This correction is significant: -12 dB for data recorded at 400 kPa and 120 K.

Figure 6 shows the sound pressure level for different static pressures at a constant temperature of 120 K. Each calculated spectrum shows peak maximum at the cylinder's vortex shedding frequency and smaller peaks arising from higher harmonics can be identified. Remarkably, the sound pressure level of the vortex shedding frequency decreases after reaching a Reynolds number of $75.3 \cdot 10^3$. For a Reynolds number of $148.4 \cdot 10^3$ the peak height at the vortex shedding frequency is considerably diminished. In this Reynolds number region the fluctuating lift coefficient decreases rapidly(17) and leads to an attenuated sound pressure level.

TESTS ON A A HALF MODEL AT ETW

Microphone Array

Based on the aforementioned PETW prototype microphone array with 12 microphones for pressurized and cryogenic, a microphone array consisting of 96 microphones was constructed. For the microphones 1/4-inch cryogenic condenser microphones of type 4944A by Brüel&Kjær were used. The variation in amplitude

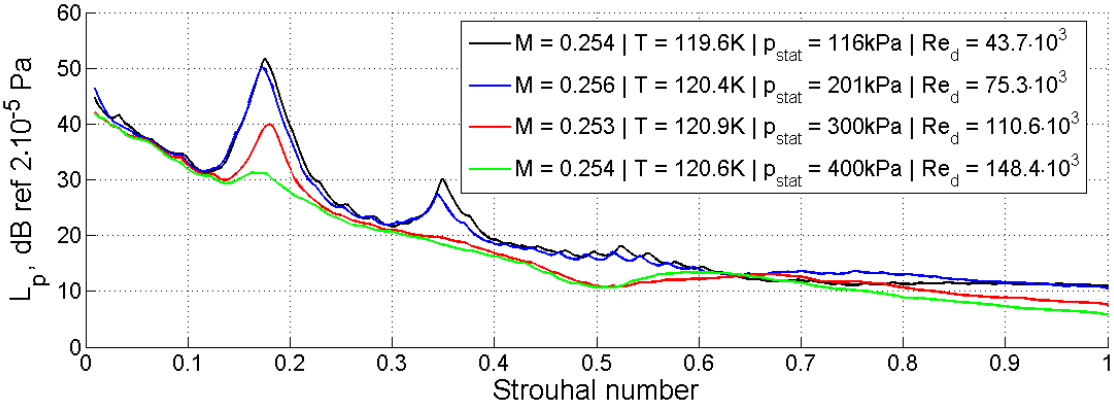

Figure 6 – Sound pressure level for several static pressures, 120 K and a Mach number 0.25. Displayed is the sound pressure level normalized to ambient conditions versus the Strouhal number.

response caused by varying the static pressure and/or the temperature was known from the previous test at the PETW.

The positioning of microphones is limited to the dummy window plates and the side wall slot inserts. Three dummy window plates and two side wall slot inserts of the test section were used for the installation of the microphones(6). The limitation for the microphone positioning leads to strong sidelobes in the beamforming procedure caused by insufficient spatial sampling. Thus, different microphones were used for the evaluation of the beamforming maps (no deconvolution applied), however all microphones were used for the calculation of deconvoluted maps. Figure 7 shows the 96 microphone positions in the (x,y)-plane.

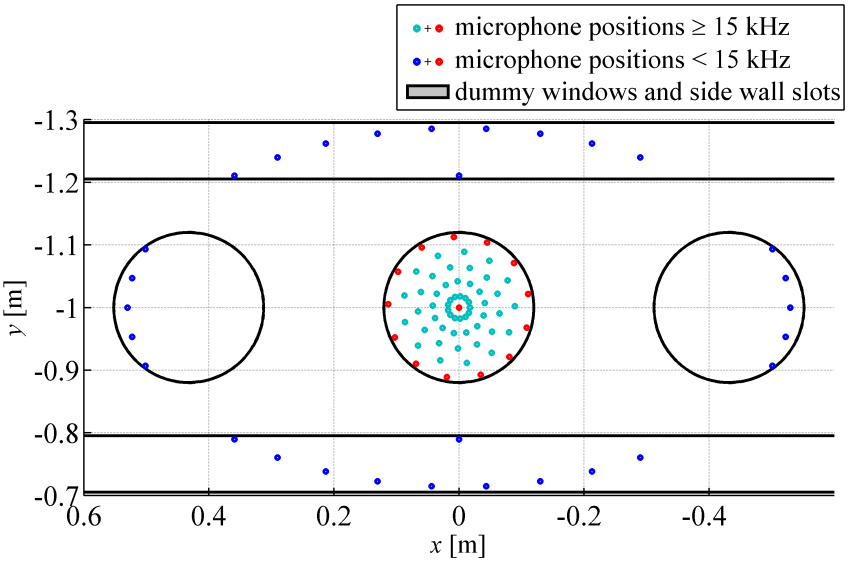

Figure 7 – Microphone positions in the (x,y)-plane viewed from outside the test section.

Measurements

The measurements were performed at the European Transonic Windtunnel ETW. The Mach number range is from 0.15 to 1.35. By injection of liquid nitrogen, the wind tunnel can be operated over a temperature range of 110 to 310 K and by pressurization, the total pressure can be varied between about 115 and 450 kPa. Thus the ETW can provide full-scale (viz. real-flight) Reynolds numbers and independent variation of Reynolds number, Mach number and load.

The Airbus K3DY half-model is located in the center of the test section and mounted on the top. The model of scale 1:13.6 is installed in landing configuration and has a half-span-width of 1.247 m and a mean aerodynamic chord length of $\delta = 0.308$ m. The model is not equipped with a landing gear and for the whole half-model no tripping device was applied. Figure 8 shows a photo of the half-model and the microphone array using the compressed laminated wood inserts in the wind tunnel side wall.

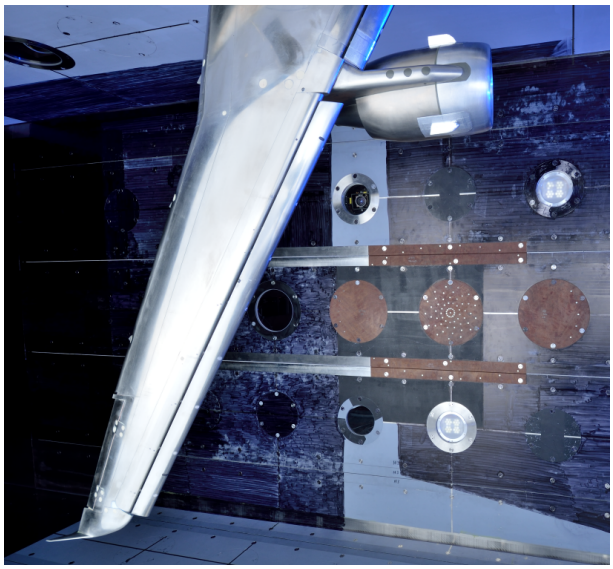

Figure 8 – Photo of the test section with the microphone array mounted into the side wall and the K3DY half-model in the center.

One important aspect is the increase of load caused by the increased total pressure. Variation of the wind tunnel pressure p_{tot} causes an increased dynamic pressure q, which has an aeroelastic effect on the wing and will deform it.
The measurements were performed at three different Reynolds numbers: $Re_\delta = 1.42 \cdot 10^6$ as a reference for standard wind tunnels, $Re_\delta = 5.16 \cdot 10^6$ as an increased Reynolds number and $Re_\delta = 20.00 \cdot 10^6$ as the real-flight Reynolds number case. The Reynolds number $5.16 \cdot 10^6$ was adjusted in two different ways: by increasing the total pressure at ambient temperature and by decreasing the temperature at ambient pressure. Taking the elastic deformation q/E into account, four points of measurement (MP I to MP IV) were chosen as shown in table 1 for a Mach number of 0.203.

Measurement	Temperature T [K]	Total pressure p_{tot} [kPa]	Reynolds number Re_δ [10^6]	Deformation q/E [10^{-8}]
MP I	310	110	1.42	1.57
MP II	125	115	5.16	1.57
MP III	310	399	5.16	5.70
MP IV	120	419	20.00	5.70

Table 1 – Flow parameter of the points of measurement MP I to MP VI for a Mach number of 0.203.

Between the measurement points MP I and MP II and MP III and MP IV, respectively, the influence of different Reynolds number at the same elastic deformation can be observed. The comparison of the points MP II and MP III shows the influence of different elastic deformation at the same Reynolds number on the aeroacoustic results. Thus the effect of the elastic deformation can be separated from the effect of the Reynolds number. Additionally, measurements were performed at Mach numbers of 0.175 and 0.225 leading to different deformations and Reynolds numbers. The angle of attack was varied from 3° to 9° for MP I to MP III and from 0° to 12° for MP IV.

Results

The source maps were computed using the beamforming method (equation 1) and the CLEAN-SC deconvolution method(16). The arbitary widths of the clean beams were set to 5 cm at 3 dB below the peak. The results are displayed as a functions of the Strouhal number St_δ.
Source maps are shown in figure 9 and 10 for a Mach number of $M = 0.203$ and an angle-of-attack of $\alpha = 3°$for different Reynolds numbers (MP I to MP IV). The sound pressure level for the results is normalized to the maximum level of MP II at $St_{1/3Oct} = 20$ with a dynamic range of 20 dB. For comparison, the maximum level

of the range is that appropriate to the maximum level for each Strouhal number band of figures 9 and 10.
Figure 9 shows the comparison of results at $Re = 1.42 \cdot 10^6$ and $5.16 \cdot 10^6$. The elastic deformation $q/E = 1.55 \cdot 10^{-8}$ is identical. In general the source maps show dominant sources at the inboard slats, the slat tracks and the flap-side edge, with less dominant sources at the flap and the flap track fairings. At a Strouhal number of 20, the comparison shows differences on the slat. For one sources on the outer slat the level is increased level by about 7 dB and several other sources on the slat show small changes in amplitude up to 3 dB. With Strouhal numbers of 90 and 130, the maps show also a different behavior. The map on the left for the lower Reynolds number shows additional dominant sources on the slat; further investigations revealed that these sources are related to narrow tonal components in the spectrum. The higher Reynolds number map show that these sources lose their dominant tonal character. Instead, an additional source of somewhat lower significance appears for a Strouhal number of 130 on the inboard flap side edge. This source was attributable to a tape which had become partly detached during the last measurement in the time schedule (MP II). The maps for a Strouhal number of 190 are similar, only that at the higher Reynolds number the overall level is increased by approximately 3 dB.
Figure 10 shows the comparison between $Re = 5.16 \cdot 10^6$ and $Re = 20 \cdot 10^6$. The elastic deformation $q/E = 5.64 \cdot 10^{-8}$ is identical. Up to a Strouhal number of 90 the comparison shows almost the same map. Small variations up to 3 dB can be found on the slat tracks and the inner slat. For a Strouhal number of 130, the source map for the real-flight Reynolds number shows differences. Sources with a significantly increased noise level appear on the inner flap and on one flap fairing, with the source level on the flap-side edge being increased by about 3 dB. The sources on the inner flap are the most dominant sources for the real-flight Reynolds number case, where the source levels on the slat are decreased by 3 dB to 5 dB. At a Strouhal number of 190 the source map for the real-flight Reynolds number again shows additional sources. They are the most dominant and can be found on the inner and outer flaps close to the flap fairings.
The effect of the different elastic deformation at the same Reynolds number can be observed by comparing MP II and MP III (figure 9 e-h vs. figure 10 a-d). For Strouhal numbers up to 90 the comparison shows almost the same map; the sound sources are almost equal in location and source strength. For higher Strouhal numbers the comparison shows in general the same map, but, nevertheless, several differences can still be observed. For the lower q/E an additional source of lower dominance appears on the inboard flap side edge (which had been attributed to a detached tape) and at a Strouhal number of 190 the overall level of the sources on the slat and the flap is increased by 3 dB to 4 dB.
To summarize the observations from the maps, two important statements can be made: First, for low Strouhal numbers up to 100 the Reynolds number and the q/E variation have only a very slight effect on the source maps. An exception to this are sources on the slat with a strong tonal character[1], which disappear with a rise of the Reynolds number. This observation has also been made by the author in a test with a half-model in a cryogenic wind tunnel facility, as mentioned previously(5). Secondly, for the real-flight Reynolds number and high Strouhal numbers additional dominant noise sources appear on the flap, possibly related to a thinner boundary layer interacting with the flap gap flow and the flap track fairings and/or the trailing edge of the wing. Based the observations made, these sources on the flap can be attributed to Reynolds number effects.

SUMMARY

This paper gives an overview over the development process of microphone array measurement technique in cryogenic and pressurized conditions to measure scaled models at real Reynolds numbers. The feasibility of the cryogenic measurement equipment has been shown on a cylinder as a known aeroacoustic source, first at cryogenic and ambient pressure conditions and second on cryogenic and pressurized conditions. With the last step the availability of the microphone array measurement technique has been demonstrated in the cryogenic and pressurized test section of the European Transonic Windtunnel (ETW) on an industrial scaled aircraft half-model. In this demonstration experiment, the sound radiation in a high-lift configuration was successfully examined from Reynolds numbers of $Re_\delta = 1.23 \cdot 10^6$ up to real-flight Reynolds numbers of $Re_\delta = 22.1 \cdot 10^6$. For Strouhal numbers up to 100 the Reynolds number and the variation of deformation have a small effect on the overall radiated airframe noise. For Strouhal numbers above 100 very significant broadband peak increases can be observed for real-flight Reynolds numbers. In order to demonstrate the suitability of aeroacoustic small-scale model measurements, it is necessary to compare the results from these tests with wind tunnel testings on a full scale model, and also, ultimately, with flyover tests.

[1] Those tones have already been investigated in experimental(18) and numerical(19) studies

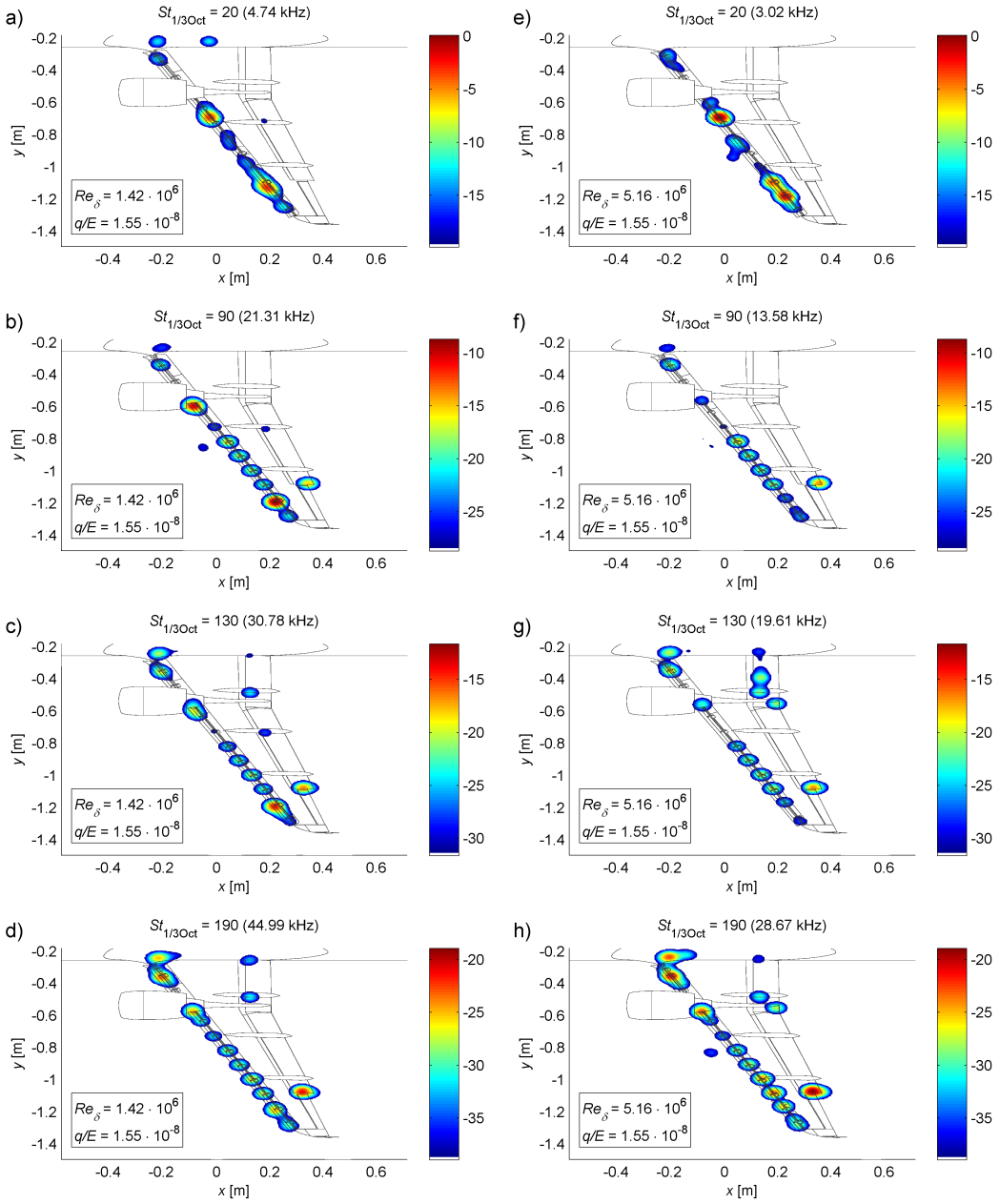

Figure 9 – Comparison of the CLEAN-SC source maps (dB) at $M = 0.203$, $\alpha = 3°$ and $q/E = 1.55 \cdot 10^{-8}$; MP I (a-d): $Re_\delta = 1.42 \cdot 10^6$; MP II (e-h): $Re_\delta = 5.16 \cdot 10^6$. Displayed are the 3rd-octave Strouhal number band results.

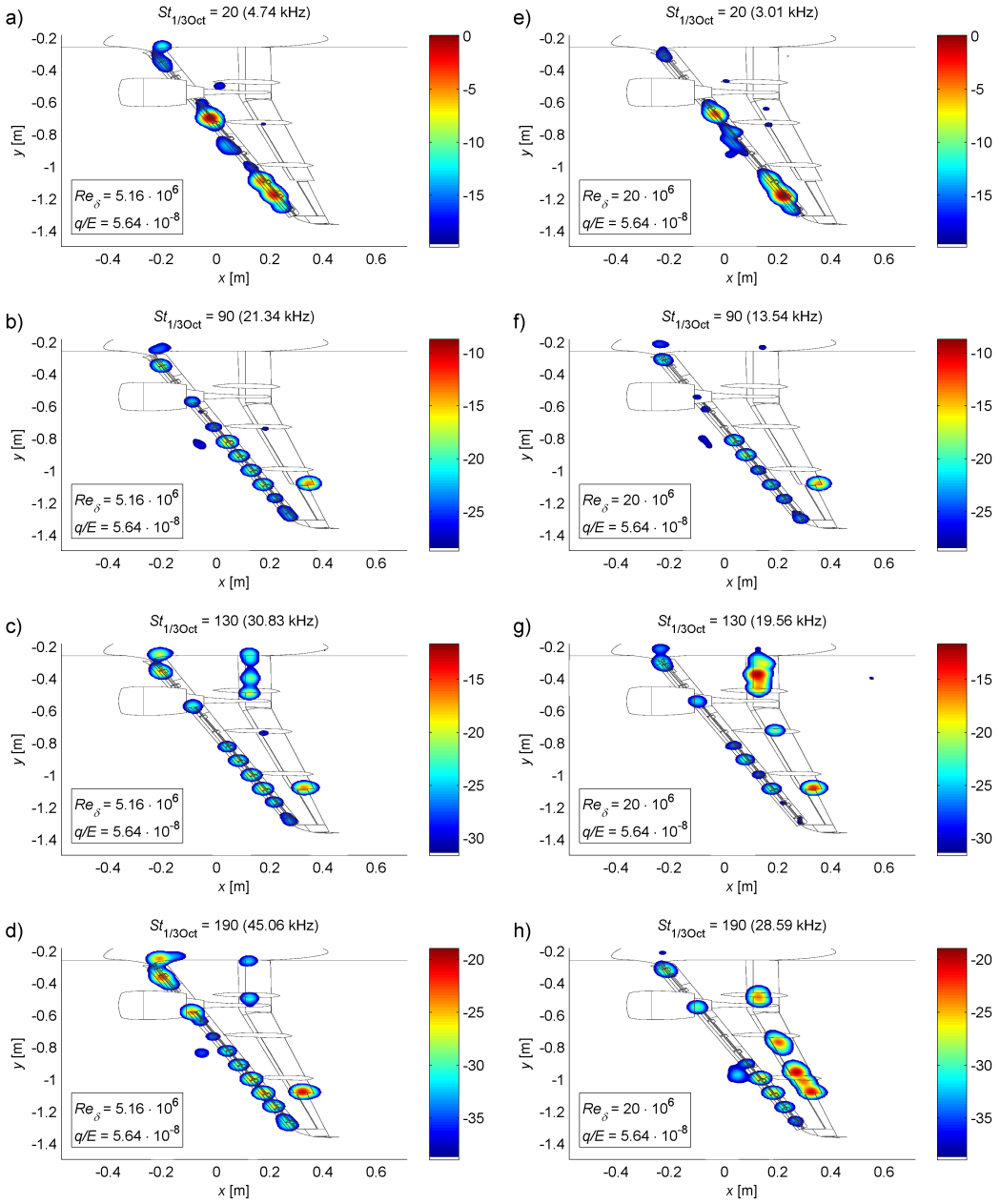

Figure 10 – Comparison of the CLEAN-SC source maps (dB) at $M = 0.203$, $\alpha = 3°$ and $q/E = 5.64 \cdot 10^{-8}$ MP III (a-d): $Re_\delta = 5.16 \cdot 10^6$; MP IV (e-h): $Re_\delta = 20 \cdot 10^6$. Displayed are the 3rd-octave Strouhal number band results.

REFERENCES

1. Stoker, R. W., Guo, Y., Street, G. and Burnside, N., "Airframe Noise Source Location of a 777 Aircraft in Flight and Comparisons with Past Model Scale Tests," *AIAA-2003-3232, 9th AIAA/CEAS Aeroacoustics Conference*, 2003.
2. Koop, L., Kröber, S., Ahlefeldt, T., Ehrenfried K. and Spehr, C., "Microphone-array Measurements in wind tunnels: Challenges and Limitations," *BeBeC 2012 - Berlin Beamforming Conference*, 2012.
3. T. Ahlefeldt and L. Koop, "Microphone Array Measurements in a Cryogenic Wind Tunnel," *AIAA-Journal*, Vol. 48, No. 7 2010, pp. 1470–1479, 2010.
4. T. Ahlefeldt and J. Quest, "High-Reynolds Number Aeroacoustic Testing Under Pressurised Cryogenic Conditions in PETW," *AIAA-2012-0107, 50th AIAA Aerospace Sciences Meeting including the New Horizons Forum and Aerospace Exposition*, 2012.
5. T. Ahlefeldt, "Aeroacoustic Measurements of a Scaled Half-Model at High Reynolds Numbers," *AIAA-Journal*, Vol. 51, No. 7 2013, pp. 2783–2791, 2013.
6. T. Ahlefeldt and J. Quest, "Real-Flight Reynolds Number Microphone-Array Measurements on a Scaled Model in ETW," *AIAA-2014-1483, 52th AIAA Aerospace Sciences Meeting*, 2014.
7. P. Sitsma, "Experimental techniques for identification and characterisation of noise sources," *Advances in Aeroacoustics and Applications*, VKI Lecture Series, 2005.
8. J. Hilsenrath, C. W. Beckett, W. S. Benedict, L. Fano, H. J.Hodge, J. F. Masi, R. L. Nuttall, Y. S. Touloukian and H. W.Woolley, *Tables of Thermal Properties of Gases*, National Bureau of Standards Circular 564, Washington D.C., 1955.
9. D. G. Crighton, "Airframe Noise," *In: NASA. Langley Research Center, Aeroacoustics of Flight Vehicles: Theory and Practice. Volume 1: Noise Sources pp. 391–447*, 1991.
10. P. T. Sodermann, F. Kafyeke, N.J. Burnside, R. Chandrasekharan, S. M. Jaeger and J. Boudreau, "Airframe noise study of a CRJ-700 aircraft model in the NASA Ames 7- by 10-Foot Wind Tunnnel No. 1," *AIAA-2002-2406, 8th AIAA/CEAS Aeroacoustics Conference and Exhibit*, 2002.
11. Y.P. Guo and M.C. Joshi, "Noise characteristics of Aircraft High Lift Systems," *AIAA-Journal*, Vol. 41 2003, pp. 1247–1256, 2003.
12. W. Dobrzynski, "Almost 40 Years of Airframe Noise Research: What Did We Achieve?," *Journal of Aircraft*, Vol. 47, No. 2 2010, pp. 353–367, 2010.
13. N. Curle, "The Influence of Solid Boundaries upon Aerodynamic Sound," *Proceedings of the Royal Society of London. Series A, Mathematical and Physical Sciences*, Vol. 231 1955, pp. 505–514, 1955.
14. Fujita, H., Suzuki, H., Sagawa, A., and Takaishi, T., "The aeolian tone characteristics of a circular cylinder in high Reynolds number flow," *5th AIAA/CEAS Aeroacoustics Conference*, 1999.
15. Norberg, C., "Fluctuating lift on a circular cylinder: review and new measurements," *Journal of Fluid and Structures*, Vol. 17 2003, pp. 57–96, 2003.
16. P. Sitsma, "CLEAN based on spatial source coherence," *International Journal of Aeroacoustics*, Vol. 6 2007, pp. 357–374, 2007.
17. Zdravkovich, M. M., editor, *Flow around circular cylinders*, Vol. 1, Oxford University Press Inc., 1997.
18. Dobrzynski, W. and Pott-Polenske, M., "Noise Source Studies for Farfield Noise Prediction," *AIAA-2001-2158, 7th AIAA/CEAS Aeroacoustics Conference*, 2001.
19. Khorrami, M. R., "Understanding Slat Noise Sources," *Colloquium EUROMECH 449*, 2003.